RESEARCH ARTICLE

Effects of Microhydration on the Mechanisms of Hydrolysis and Cl^- Substitution in Reactions of N_2O_5 and Seawater

Laura M. McCaslin[a]*, Andreas W. Götz[b], Mark A. Johnson[c], and R. Benny Gerber[d,e]*

[a] Dr. L.M. McCaslin
Combustion Research Facility
Sandia National Laboratories
Livermore, CA 94550 (USA)
lmmccas@sandia.gov
[b] Dr. A.W. Götz
San Diego Supercomputer Center
University of California San Diego
La Jolla, CA, 92093 (USA)
[c] Prof. M.A. Johnson
Department of Chemistry
Yale University
New Haven, CT 06525 (USA)
[d,e] Prof. R.B. Gerber
Institute of Chemistry and the Fritz Haber Center for Molecular Dynamics
The Hebrew University
Jerusalem 9190401 (IL)
Department of Chemistry
University of California Irvine
Irvine, CA 92597 (USA)
benny@fh.huji.ac.il

Supporting information for this article is given via a link at the end of the document.

Abstract: The reaction of N_2O_5 at atmospheric interfaces has recently received considerable attention due to its importance in atmospheric chemistry. N_2O_5 reacts preferentially with Cl^- to form $ClNO_2/NO_3^-$ (Cl^- substitution), but can also react with H_2O to form $2HNO_3$ (hydrolysis). In this paper, we explore these competing reactions in a theoretical study of the clusters $N_2O_5/Cl^-/nH_2O$ (n=2-5), resulting in the identification of three reaction motifs. First, we uncovered an S_N2-type Cl^- substitution reaction of N_2O_5 that occurs very quickly due to low barriers to reaction. Second, we found a low-lying pathway to hydrolysis via a $ClNO_2$ intermediate (two-step hydrolysis). Finally, we found a direct hydrolysis pathway where H_2O attacks N_2O_5 (one-step hydrolysis). We find that Cl^- substitution is the fastest reaction in every cluster. Between one-step and two-step hydrolysis, we find that one-step hydrolysis barriers are lower, making two-step hydrolysis (via $ClNO_2$ intermediate) likely only when concentrations of Cl^- are high.

Introduction

The reactive uptake of N_2O_5 to sea spray aerosols has been described as "the dominant heterogeneous reaction in the troposphere"(*1*) due to its influence on global levels of key atmospheric compounds.(*1*–*7*) Model studies indicate that changes in this reactive uptake of N_2O_5 on sea spray aerosols can affect levels of OH, O_3, and NO_x by up to 15%, 12%, and 25%, respectively.(*1*, *8*, *9*) Moreover, it has been determined that N_2O_5 uptake is determined by interfacial and near-interfacial features, with hydrolysis occurring within 2 nm of the aqueous surface due to an interplay of reactivity and interfacial adsorption free energy.(*10*) Recent studies are beginning to unravel the mechanisms of many types of reactions that N_2O_5 can undergo at the surface of sea spray aerosols, including reactions with H_2O, Cl^-, SO_4^{2-}, NH_3, and ClO_4^-.(*11*–*16*) Two major competing reactions of N_2O_5 on halide-containing aerosols are hydrolysis and chloride substitution, forming HNO_3 and $ClNO_2$, respectively.(*7*, *17*–*19*) Formation of HNO_3 from N_2O_5 is one of the major sinks of NO_x species in the atmosphere(*1*, *2*, *7*, *20*–*23*) and photolysis of $ClNO_2$ provides a major source of reactive chlorine radicals in the atmosphere.(*24*, *25*) The competition and relative yields of these reactions thus have important implications for the chemical makeup of the atmosphere, which in turn influence radiative forcing and global climate.(*26*)

Recent studies suggest that the reactive uptake of N_2O_5 changes dramatically based on the chemical composition of the interfacial region. (*27*–*31*) Interestingly, there is increasingly strong evidence that the reactive uptake of N_2O_5 on Cl^--containing water is roughly constant with change in Cl^- concentration, opening key questions on the competition between Cl^- substitution and hydrolysis of N_2O_5 in the interfacial and near-interfacial regions of aqueous aerosol.(*23*, *32*–*37*) N_2O_5 reacts readily with H_2O and ions such as Cl^-, and SO_4^{2-} with relative product yields that are dependent on the local concentrations at the surface.(*12*, *14*) Surfactant molecules on the surface of sea spray aerosols affect the reactive uptake of N_2O_5 in complex ways depending on the local chemical composition and structure. Long alkyl chains can impede the entry of N_2O_5 and other gasses.(*4*, *5*, *38*, *39*) However, organic surfactants can also increase N_2O_5 reactivity by adding reactive sites and pulling reactive ions to the surface.(*29*) Molecules such as phenol can also undergo direct reaction with N_2O_5.(*39*) Although the complexity of the interfacial chemistry at play in ambient aerosol presents a daunting challenge for theory, several recent reports have shed light on critical factors controlling reaction pathways by carrying out electronic structure calculations on smaller model systems that isolate water molecules, ions, and N_2O_5 interactions.(*11*–*14*) One key issue that emerges from these earlier studies on the reactivity of N_2O_5 with H_2O and Cl^- is the clarification of how the reactive mechanisms depend on the number of local water molecules.(*16*) Here we present the results of a theoretical study that elucidates how the degree of hydration changes the potential energy landscape underlying the various reaction pathways that occur in the $N_2O_5/Cl^-/nH_2O$ (n=2-5) clusters.

The reaction pathways at play in interaction of N_2O_5 with

halides in small water clusters have been explored experimentally by Kelleher et al. who measured the vibrational spectra of the $X^-{\cdot}N_2O_5$ products using a cryogenic photofragmentation mass spectrometer. (*40*) Analysis of the resulting bands established that these species are the "exit channel" ion-molecule complexes of the general form $[NO_3^-{\cdot}XNO_2]$ (X = Cl, Br, I). Formation and isolation of the XNO_2 products indicates that N_2O_5 preferentially undergoes halide substitution over hydrolysis in small water clusters. One open question left unanswered from that study is the determination of the number of water molecules in the $X^-{\cdot}nH_2O$ clusters that generate the binary $[NO_3^-{\cdot}XNO_2]$ ion-molecule complex. This uncertainty raises the question of how the number of water molecules affects the relative probability of the N_2O_5 halide substitution and hydrolysis reactions. Further experimental and theoretical study of $N_2O_5/Cl^-/nH_2O$ (n=2-5) is thus required to establish the fundamental mechanism that drives N_2O_5 uptake and reactivity in this simple model system.

A recent theoretical study on the competition between Cl^- substitution and hydrolysis of the ternary $N_2O_5/Cl^-/H_2O$ system identified key features of the potential energy surface (PES) along key intrinsic reaction coordinates (IRC) as well as explored the dynamics at play at elevated temperature with *ab initio* molecular dynamics simulations (AIMD). (*11*) It was found that the Cl^- substitution reaction of N_2O_5 to form $ClNO_2$ is almost barrierless (0.6 kcal/mol) and thus occurs very quickly. Additionally, the mechanism of Cl^- substitution was shown to feature many characteristics of S_N2 reactions, including concerted nucleophilic attack and presence of $NO_3^{\delta-}$ leaving group. The competing hydrolysis reaction was determined to be significantly enhanced by the presence of Cl^-, lowering the barrier by approximately 15 kcal/mol compared to the barrier to hydrolysis in the neutral $N_2O_5/2H_2O$ system.(*41*) Here we report the results of a theoretical study that determines how the $Cl^-/N_2O_5/nH_2O$ cluster structures and barriers to hydrolysis and substitution evolve with increasing numbers of water molecules in the range n=1-5. Furthermore, the calculated partial charges along the reaction pathways shed light on the differing responses of the S_N2-type halide substitution reaction and the competing hydrolysis reaction to the dominant microsolvation environments.

Results and Discussion

The three distinct reaction pathways at play in the $N_2O_5/Cl^-/nH_2O$ clusters are:

Halide substitution:

$$N_2O_5/Cl^-/nH_2O \rightarrow ClNO_2/NO_3^-/nH_2O \quad (1)$$

$ClNO_2$ - mediated hydrolysis:

$$ClNO_2/NO_3^-/nH_2O \rightarrow HNO_3/NO_3^-/HCl/(n\text{-}1)H_2O \quad (2)$$

Direct hydrolysis:

$$N_2O_5/Cl^-/nH_2O \rightarrow HNO_3/NO_3^-/HCl/(n\text{-}1)H_2O \quad (3)$$

The TS motifs identified for these reactions were embedded in larger clusters and reoptimized to follow how the corresponding TS structures and energies evolve as a function of cluster size. A root mean squared deviation (RMSD) analysis of the geometric structures of the TS motifs or substructures (terms used interchangeably in this work) is employed to verify that these TS substructures are preserved as the clusters grow in size. We note that the identification of such TS substructures and analysis of their changes upon subsequent addition of water molecules is important beyond the present cluster study as they can inform larger-scale studies of these reactions in condensed phase, as as well as the basis for understanding the reactive motifs of N_2O_5, Cl^- and H_2O. Figure 1 presents the three TS

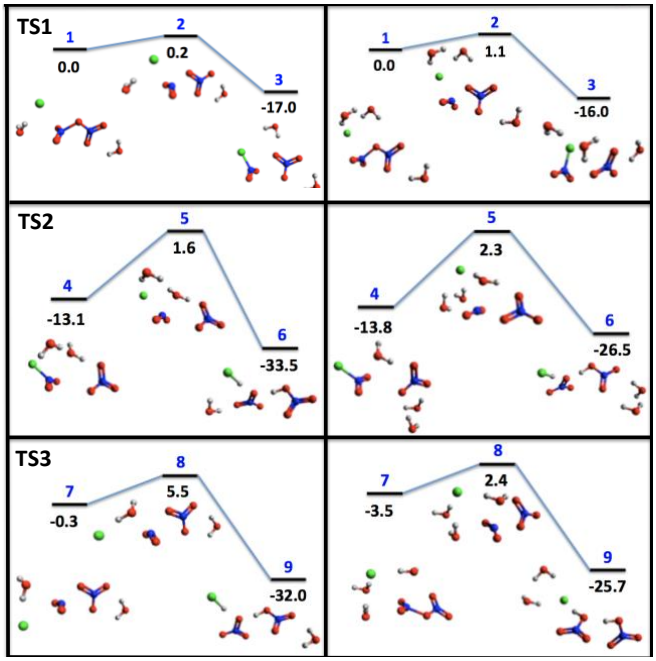

Figure 1. Left: Lowest-lying IRC pathways from n=2 clusters that contain the TS motif. Right: Corresponding lowest-lying IRC pathways from n=3 clusters. Top: TS1 corresponds to the $N_2O_5/Cl^-/nH_2O \rightarrow ClNO_2/NO_3^-/nH_2O$ reaction; Middle: TS2 corresponds to the $ClNO_2/NO_3^-/nH_2O \rightarrow HNO_3/NO_3^-/HCl/(n\text{-}1)H_2O$ reaction; Bottom: TS3 corresponds to the $N_2O_5/Cl^-/nH_2O \rightarrow HNO_3/NO_3^-/HCl/(n\text{-}1)H_2O$ reaction. Relative energies (kcal/mol) are reported with respect to the $N_2O_5/Cl^-/nH_2O$ cluster with lowest barrier to Cl- substitution.

substructures identified for the n=2-5 clusters in this work, which are shown for the smaller n=2 and 3 clusters for clarity. TS1 is defined as the TS between $N_2O_5/Cl^-/nH_2O$ and $ClNO_2/NO_3^{\delta-}/nH_2O$ that governs Cl^- substitution. TS2 is defined as the TS between $ClNO_2/NO_3^-/nH_2O$ and $HNO_3/NO_3^-/HCl/(n\text{-}1)H_2O$, which corresponds to H_2O displacement of Cl^- in $ClNO_2$ to yield HNO_3, i.e. $ClNO_2$-mediated hydrolysis. TS3 is defined as the TS between $N_2O_5/Cl^-/nH_2O$ and $HNO_3/NO_3^-/HCl/(n\text{-}1)H_2O$. This corresponds to H_2O attack on N_2O_5, which is direct hydrolysis without the explicit participation of the Cl^- ion. The left and right panels in Figure 1 are meant for comparison: each transition state motif within the n=2 and n=3 clusters is structurally similar (thus characterized by a low RMSD value as defined in the following paragraphs).

In order to analyze the similarities of the geometries of the TS substructures (TS1-3) to the forms adopted in the fully reoptimized TS structures in the larger clusters, the RMSD analysis of the substructure geometry in the internal coordinates (defined in SI) was calculated for each TS identified with averages reported in Table 1. The reference structures for each reaction motif are taken as the lowest energy TS from the smallest cluster in which the TS is identified. This means that the reference structures for TS1 and TS2 are taken from the n=1 cluster. (*11*) Because n=2 is the smallest cluster with a stable transition state for direct attack of water on N_2O_5, TS3 is taken as the lowest-lying TS for H_2O attack in n=2. In each case reported, the RMSD in bond length is very low (under 0.10 Å for H_2O or Cl^- attack on N_2O_5 and under 0.25 Å for displacement of Cl^- by H_2O). The RMSD for the angles and dihedral angles is under 41° for each The larger deviations in angles and dihedrals (compared to bond length deviations) are largely due to fluctuations in the angle and dihedral angles that describe the relative orientation of the $NO_2^{\delta+}$ and $NO_3^{\delta-}$ moieties. Under this analysis, we can conclude that the molecular and ionic moieties retain similar geometries across the clusters sampled. More

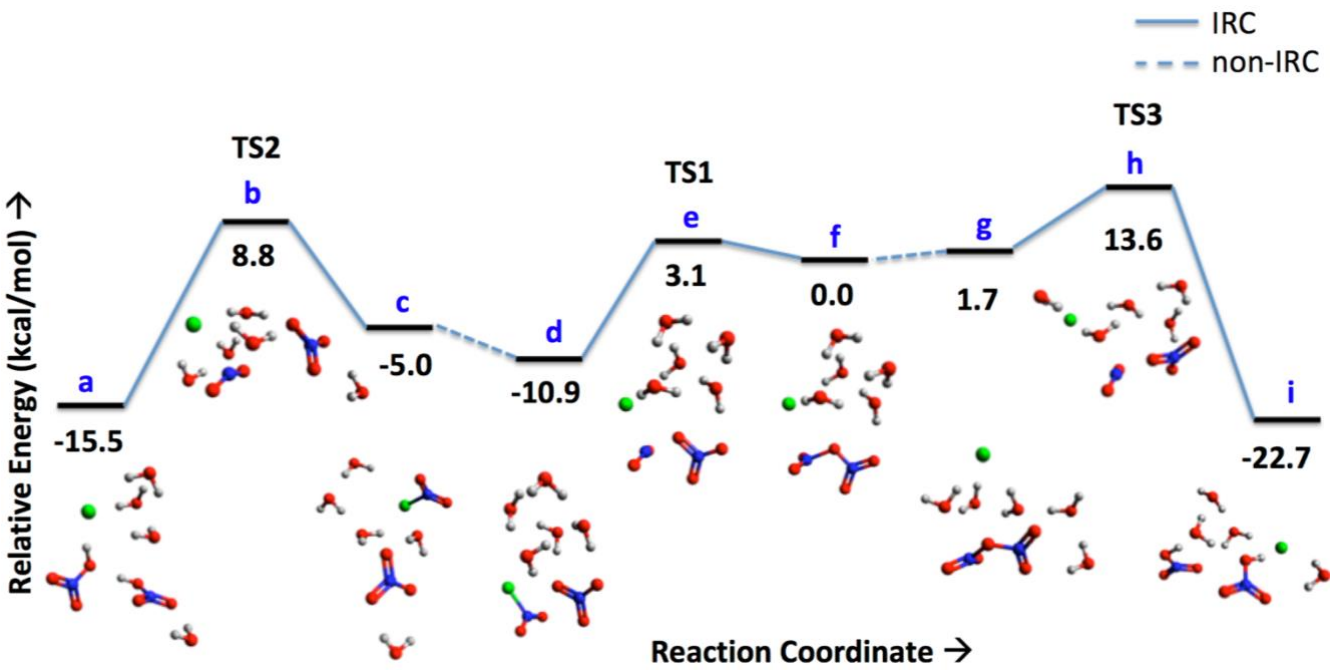

Figure 2. Reaction mechanisms of $N_2O_5/Cl^-/5H_2O$. Indices f and g both represent intact $N_2O_5/Cl^-/5H_2O$. Index h corresponds to substructure TS3 (direct attack of H_2O on N_2O_5). Index e corresponds to substructure TS1 (direct attack of Cl^- on N_2O_5). Index b corresponds to substructure TS2 displacement of Cl^- by H_2O in $ClNO_2$).

interestingly, the geometric parameters related to the orientations between these molecular moieties are preserved across a variety of cluster sizes and energies.

The RMSD analysis of the TS geometries provides many key insights. First, we show that the two TS substructures (**TS1**, **TS2**) identified in the n=1 cluster are preserved upon the addition of water molecules. This allows for extrapolation of structural insights gained at the cluster level to larger studies of seawater interfaces, as the reactive TS structures are shown to be preserved. Secondly, we have identified a new motif for reaction: direct H_2O attack of N_2O_5 (**TS3**), which was not identified in the n=1 cluster, but emerges in n=2 and appears as a shared motif in all clusters from n=3 to n=5. The TS substructures identified here capture the nature of the reactions of N_2O_5 with water and chloride at a microscopic level. They additionally build a framework for studying the reactions of N_2O_5 with Cl^- and H_2O at interfaces.

We now turn to the size dependence of the barriers to each reaction. The previous study of the n=1 $N_2O_5/Cl^-/H_2O$ cluster identified two TS structures (**TS1**, **TS2**) and reported barriers with respect to their adjacent minima determined from calculations of the IRC.(*9*) As in the previous study, IRCs were computed and validated for each of the TS structures reported here. We report in Table 2 the lowest barrier energy found for each of the 3 reaction motifs, where the barrier height energy is reported as the difference between the TS energy and energy of adjacent minimum, as reported in our previous study.

As shown in Table 2, the lowest-lying barriers in the n=2-5 clusters are those for the Cl^- attack on intact N_2O_5 (**TS1 reaction**), where all barriers are between 0.2 and 3.1 kcal/mol and increase monotonically with system size. The next lowest barriers correspond to direct hydrolysis of N_2O_5, or the one-step hydrolysis mechanism (**TS3** reaction), where barriers are found to be ~5.5 kcal/mol for n=2-4 and 11.8 kcal/mol for n=5. In comparing nucleophilic attack of Cl^- vs H_2O on N_2O_5, the barriers to reaction by Cl^- are small significantly lower than that of H_2O, indicating that Cl^- will react with N_2O_5 readily when Cl^- ions are present and nearby. Of the three reaction motifs, the highest barriers correspond to displacement of Cl^- by H_2O in $ClNO_2$ (**TS2**), known as step two in the two-step, Cl^--mediated mechanism to hydrolysis. From these results, we predict that when N_2O_5 is in the proximity of Cl^- in water, $ClNO_2$ will readily form via nucleophilic attack of Cl^- on N_2O_5. If $ClNO_2$ remains at the sea water interface, it can undergo hydrolysis via the two-step mechanism (displacement of Cl^- by H_2O). Alternatively, when Cl^- is not adjacent to N_2O_5, direct hydrolysis via attack of H_2O on N_2O_5 is expected to occur. Large scale dynamical studies that investigate the effects of Cl^- proximity to N_2O_5 on hydrolysis mechanisms are needed to unravel these competitive pathways, but are outside the scope of this paper.

The dependence of the various barrier heights on the arrangement and number of proximal water molecules indicates the importance of the hydrogen bonding microenvironment in which N_2O_5 reacts. For example, a molecular dynamics study(*42*) of N_2O_5 on the surface of pure bulk revealed that, even though it does not undergo hydrolysis, N_2O_5 displays significant intramolecular charge fluctuations of approximately -0.05 to -0.3 a.u. A study by Hammerich et al. reported that large fluctuations in the charge distribution of N_2O_5 greatly affect reactivity with Cl^- in water.(*43*) In this context, we note that the

Table 1. Average RMS deviations from reference TS substructures

n	TS1: $N_2O_5/Cl^- \rightarrow ClNO_2/NO_3^-$			TS2: $ClNO_2/NO_3^-/H_2O \rightarrow HNO_3/NO_3^-/HCl$			TS3: $N_2O_5/H_2O \rightarrow 2HNO_3$		
	Bond RMSD (Å)	Angle RMSD (°)	Dihedral RMSD (°)	Bond RMSD (Å)	Angle RMSD (°)	Dihedral RMSD (°)	Bond RMSD (Å)	Angle RMSD (°)	Dihedral RMSD (°)
2	0.04	1.27	0.91	0.06	13.57	34.97	0.03	19.42	23.43
3	0.04	1.88	1.69	0.12	14.92	40.86	0.04	9.40	20.19
4	0.10	10.08	10.75	0.13	16.51	40.54	0.03	5.97	13.14
5	0.07	7.51	11.05	0.25	21.83	33.85	0.02	26.14	33.92

partial charge separation in the TS structures of the n=5 cluster (see Figure 2), reveals the role of stabilizing hydrogen bonds between water and $NO_2^{\delta+}$ and $NO_3^{\delta-}$ moieties . The cluster size dependence of the charges on the Cl^-, NO_2 and NO_3 constituents is reported in Table 3.

The study of the reactions of the n=1 $N_2O_5/Cl^-/H_2O$ cluster compared the energetic barrier to hydrolysis with that of the neutral $N_2O_5/2H_2O$ cluster.(*11*) It was found that the presence of Cl^- lowers the barrier to hydrolysis by ~15 kcal/mol.(*44*) While other studies have explored the reactions of N_2O_5/nH_2O with varying number of water molecules, there is not data in the literature that allows for direct comparison to this work for n=2-5. However, one study calculated a (non-ZPE corrected) barrier to hydrolysis of $N_2O_5/6H_2O$ to be 4.1 kcal/mol.(*45*) If we calculate the non-ZPE corrected barrier to hydrolysis in the lowest-lying n=5 cluster (see Figure 2), the barrier to hydrolysis is 11.5 kcal/mol (and 11.8 kcal/mol with ZPE correction). This indicates that if the Cl^- is replaced by H_2O in the n=5 system, the barrier to hydrolysis is ~7 kcal/mol lower in energy. While a direct comparison is only approximate due to differences in the level of theory and lack of ZPE data, the evidence is clear that the local presence of Cl^- raises the barrier to direct hydrolysis substantially. A primary reason for this is that Cl^- strengthens the hydrogen bonds between the water molecules, creating an additional energetic penalty for H_2O to attack $NO_2^{\delta+}$. Further comparison of the energetic barriers to hydrolysis in the presence vs. absence of ions will offer deeper insights into the effects of the microenvironment on the reactive yields of N_2O_5.

Table 2. Lowest barriers to Cl^- substitution and hydrolysis (in kcal/mol) in clusters of $N_2O_5/Cl^-/nH_2O$ (n=2-5). Column 2 represents barriers to Cl^- substitution. Column 3 represents barrier to displacement of Cl^- by H_2O in $ClNO_2$. Column 4 represents barrier to H_2O attack on N_2O_5.

n	**TS1:** $N_2O_5/Cl^-/nH_2O \rightarrow ClNO_2/NO_3^-/nH_2O$	**TS2:** $ClNO_2/NO_3^-/nH_2O \rightarrow HNO_3/NO_3^-/HCl/(n-1)H_2O$	**TS3:** $N_2O_5/Cl^-/nH_2O \rightarrow HNO_3/NO_3^-/HCl/(n-1)H_2O$
2	0.2	14.6	5.8
3	1.1	16.0	5.6
4	2.3	13.8	5.3
5	3.1	13.9	11.8

In studying the S_N2 nature of the Cl^- substitution reaction, the extent of charge transfer from the attacking Cl to the NO_3 leaving group is of key interest. Table 3 presents the changes in partial charge of the Cl, NO_2, and NO_3 between the intact reactant $N_2O_5/Cl^-/nH_2O$ and product $ClNO_2/NO_3^-/nH_2O$ minima. In each case, the magnitude of charge on Cl is over 0.88 in the intact $N_2O_5/Cl^-/nH_2O$ cluster, showing that negative charge is localized on the Cl before attack of N_2O_5. At the minimum for the intact $N_2O_5/Cl^-/nH_2O$ cluster, the NO_3 charges range from -0.25 to -0.46, with corresponding positive charges on the NO_2 moiety. In all cases, the NO_2 and NO_3 charges sum to a magnitude less than 0.04 a.u. Upon reaction to form $ClNO_2/NO_3^-/nH_2O$, both the Cl and NO_2 have small charges with magnitude under 0.07 a.u. The NO_3, however, has negative charge with magnitude over 0.9, showing that upon substitution, the localized Cl charge in the intact $N_2O_5/Cl^-/nH_2O$ clusters transfers completely to the NO_3^- leaving group. This change in charge localization is reminiscent of charge transfer seen in traditional S_N2 reactions and may be used as a metric in future studies of S_N2-type reactions of atmospheric nitrogen oxides and ions.

In order to quantify the bond formation times in n=2-5 clusters for comparison to the n=1 cluster, AIMD calculations initialized at each of the 3 TSs were performed. Tables 1-4 in the SI represent average bond formation times derived from AIMD calculations initialized at all TSs reported. Average Cl-N bond formation time from **TS1** and **TS2** are reported to be between 80.9 and 111.8 fs. The previous work reports that the Cl-N bond formation time from each TS is on the order of the vibrational period of Cl-N, which is ~90 fs.(*46*) All positive deviations (i.e. longer timescales) from this number can be attributed to a greater energy difference between transition state energy and adjacent minimum (and vice versa), as our calculations are performed in the microcanonical (fixed energy) ensemble. The previous work reports that the O-N bond formation time from **TS2** is ~2.5x the vibrational period of the asymmetric stretch of NO_3^- (~25 fs) due to the complexity of rearrangement of bonding, including breaking an O-H bond in water and other proton transfer interactions. The AIMD studies here indicate O-N bond formation times from **TS2** and **TS3** to range from 2.5-4x this vibrational period, ranging from 67-102 fs, which accounts for molecular rearrangement in addition to formation of the O-N bond.

Table 3. Change in charges of Cl, NO_2, and NO_3 between $N_2O_5/Cl^-/nH_2O$ and $ClNO_2/NO_3^-/H_2O$ minima

n	Cl charge	NO_2 charge	NO_3 charge
2	-0.91 -> -0.07	0.43 -> 0.07	-0.46 -> -0.94
3	-0.90 -> 0.00	0.37 -> 0.00	-0.40 -> -0.92
4	-0.88 -> -0.01	0.26 -> 0.01	-0.25 -> -0.93
5	-0.89 -> -0.03	0.30 -> 0.02	-0.31 -> -0.91

Conclusion

In studying the competition between Cl^- substitution and hydrolysis of N_2O_5 in small water clusters (n=2-5 H_2O), Cl^- substitution is predicted to be much faster than hydrolysis in all cases due to relatively low barriers to reaction. In all n=2-5 clusters, the lowest lying pathway to hydrolysis occurs in a one-step process, where N_2O_5 undergoes direct attack of H_2O, which has not been shown to occur in the n=1 cluster.(*11*) Each cluster n=2-5 was found to have an S_N2-type Cl^- attack mechanism. In the n=1 cluster it was found that Cl^- acts as a catalyst to two-step hydrolysis, lowering the barrier to reaction by ~15 kcal/mol, as compared to one-step hydrolysis for n=2. Upon inclusion of the important one-step hydrolysis mechanism into the reaction picture of N_2O_5, we investigate the effect of the presence of Cl^- on the hydrolysis barrier by comparing to N_2O_5 clustered with water alone. We approximate that the barrier to hydrolytic attack of N_2O_5 in $N_2O_5/Cl^-/5H_2O$ is ~7 kcal/mol higher in energy than in the $N_2O_5/6H_2O$ cluster, meaning that Cl^- inhibits one-step hydrolysis for clusters of this size. This Cl^- induced inhibition of direct hydrolysis competes with Cl^- substitution at increasing Cl^- concentrations. All reaction times calculated by AIMD simulations were found to be on the orders of magnitude reported in previous studies.(*11*) We find that increased solvation increases barriers to Cl^- substitution, decreases barriers to two-step hydrolysis, and increases barriers to one-step direct hydrolysis. However, all reactive TSs identified shared characteristics of one of three TS motifs, which can help guide further studies that embed these motifs in complex environments, for instance molecular dynamics simulations using reactive neural network potentials in bulk liquid or at the liquid/vapor interface.

Computational Section

For each cluster and substructure, 20 guess TS structures were generated with the code Packmol (*47*) using the identified TS substructures (**TS1-3 in Figure 1**) as a molecule and “packing”

the remaining components around the substructure, generating 60 guess structures for each cluster size n=2-5, 240 structures in total. Minima and TS geometries for each cluster were calculated with the long-range corrected ωB97X-D density functional and the aug-cc-pVDZ basis set.(*48*–*50*) Single point energy calculations were performed for these geometries at the CCSD(T) level using frozen natural orbitals (FNO) and density fitting (DF) for both SCF and CCSD, employing the aug-cc-pVDZ basis set.(*50*–*53*) All relative energies reported are zero-point energy corrected in the harmonic approximation at the ωB97X-D/aug-cc-pVDZ level of theory. IRCs are computed as described by Fukui.(*54*) All partial charges shown are calculated using Natural Bond Order (NBO) theory.(*55*, *56*)

AIMD is calculated at the ωB97X-D/aug-cc-pVDZ level of theory. Initial geometries are TS structures (from motifs **TS1**, **TS2**, and **TS3**) for each of the clusters n=2-5. For each transition state, 20 trajectories are calculated (240 trajectories in all) with initial velocities sampled from a Boltzmann distribution at 300K. All trajectories are calculated with a time step of 0.2 fs for a total time of 2 ps. All calculations reported here are performed with Q-Chem(*57*) except the FNO-DF-CCSD(T) calculations, which are performed with Psi4.(*58*)

Acknowledgements

The authors would like to thank Prof. Gilbert Nathanson, Prof. Tim Bertram, and Dr. David Osborn for helpful comments. This work was supported by the U.S. National Science Foundation Center for Aerosol Impacts on Chemistry of the Environment (NSF-CAICE), CHE-1801971, and XSEDE allocation TG-CHE170064. L.M.M. was supported by the Zuckerman STEM Leadership Program at The Hebrew University, NSF-CAICE at University of California Irvine, and the Division of Chemical Sciences, Geosciences and Biosciences, Office of Basic Energy Sciences (BES), U.S. Department of Energy (USDOE). Sandia National Laboratories is a multi-mission laboratory managed and operated by National Technology and Engineering Solutions of Sandia, LLC., a wholly owned subsidiary of Honeywell International, Inc., for the U.S. Department of Energy's National Nuclear Security Administration under Contract No. DE-NA-0003525. This paper describes objective technical results and analysis. Any subjective views or opinions that might be expressed in this paper do not necessarily represent the views of the U.S. Department of Energy or the United States Government.

Supporting Data: All structures reported in this manuscript can be accessed in the following data repository: https://doi.org/10.5281/zenodo.7178264

Keywords: Atmospheric Chemistry • Atmospheric Aerosols • S_N2 Reaction • Ab Initio Molecular Dynamics • Molecular Clusters

1. H. L. MacIntyre, M. J. Evans, *Atmos. Chem. Phys.* **2010**, *10*, 7409–7414.
2. X. Tie, G. Brasseur, L. Emmons, L. Horowitz, D. Kinnison, *J. Geophys. Res. Atmos.* **2001**, *106*, 22931–22964.
3. W. L. Chang, P. V. Bhave, S. S. Brown, N. Riemer, J. Stutz, D. Dabdub, *Aerosol Sci. Technol.* **2011**, *45*, 665–695.
4. S. S. Brown, J. Stutz, *Chem. Soc. Rev.* **2012**, *41*, 6405–6447.
5. J. P. D. Abbatt, A. K. Y. Lee, J. A. Thornton, *Chem. Soc. Rev.*, **2012**, *41*, 6555–6581.
6. R. B. Gerber, M. E. Varner, A. D. Hammerich, S. Riikonen, G. Murdachaew, D. Shemesh, B. J. Finlayson-Pitts, *Acc. Chem. Res.* **2015**, *48*, 399–406.
7. E. E. McDuffie, D. L. Fibiger, W. P. Dube, F. Lopez-Hilfiker, B.H. Lee, J. A. Thornton, V. Shah, L. Jaegle, H. Guo, R. J. Weber, J. M. Reeves, A. J. Weinheimer, J. C. Schroder, P. Campuzzano-Jost, J. L. Jimenez, J. E. Dibb, P. Veres, C. Ebben, T. L. Sparks, P. J Wooldridge, R. C. Cohen, R. S. Hornbrook, E. C. Apel, T. Campos, S. R. Hall, K. Ullmann, S. S. Brown, *J. Geophys. Res. Atmos.* **2018**, *123*, 4345–4372.
8. C. D. Holmes, T. H. Bertram, K. L. Confer, K. A. Graham, A. C. Ronan, C. K. Wirks, V. Shah, *Geophys. Res. Lett.* **2019**, *46*, 4980–4990.
9. B. Alexander, T. Sherwen, C. D. Holmes, J. A. Fisher, Q. Chen, M. J. Evans, P. Kasibhatla, *Atmos. Chem. Phys.* **2020**, *20*, 3859–3877.
10. V. W. D. Cruzeiro, M. Galib, D. T. Limmer, A. W. Götz, *Nat. Commun.* **2022**, *13*, 1266.
11. L. M. McCaslin, M. A. Johnson, R. B. Gerber, *Sci. Adv.* **2019**, *5*, eaav6503.
12. S. Staudt, J. R. Gord, N. V. Karimova, E. E. McDuffie, S. S. Brown, R. B. Gerber, G. M. Nathanson, T. H. Bertram, *ACS Earth Sp. Chem.* **2019**, *3*, 1987–1997.
13. S. Sarkar, B. Bandyopadhyay, *Phys. Chem. Chem. Phys.* **2021**, *23*, 6651–6664.
14. N. V. Karimova, J. Chen, J. R. Gord, S. Staudt, T. H. Bertram, G. M. Nathanson, R. B. Gerber, *J. Phys. Chem. A*. **2020**, *124*, 711–720.
15. E. Rossich Molina, R. B. Gerber, *J. Phys. Chem. A*. **2019**, *124*, 224-228.
16. S. J. Kregel, T. F. Derrah, S. J. Moon, D. T. Limmer, G. M. Nathanson, T. H. Bertram, 2022, 10.26434/chemrxiv-2022-5xr00-v2.
17. B. J. Finlayson-Pitts, M. J. Ezell, J. N. Pitts, *Nature*. **1989**, *337*, 241–244.
18. H. D. Osthoff, J. M. Roberts, A. R. Ravishankara, E. J. Williams, B. M. Lerner, R. Sommariva, T. S. Bates, D. Coffman, P. K. Quinn, J. E. Dibb, H. Stark, J. B. Burkholder, R. K. Talukdar, J. Meagher, F. C. Fehsenfeld, S. S. Brown, *Nat. Geosci.* **2008**, *1*, 324–328.
19. J. M. Roberts, H. D. Osthoff, S. S. Brown, A. R. Ravishankara, D. Coffman, P. Quinn, T. Bates, *Geophys. Res. Lett.* 2009, 36, L20808.
20. F. J. Dentener, P. J. Crutzen, *J. Geophys. Res.* **1993**, *98*, 7149–7163.
21. M. J. Evans, D. J. Jacob, *Geophys. Res. Lett.* **2005**, *32*, L09813.
22. S. S. Brown, T. B. Ryerson, A. G. Wollny, C. A. Brock, R. Peltier, A. P. Sullivan, R. J. Weber, W. P. Dube, M. Trainer, J. F. Meagher, F. C. Fehsenfeld, A. R. Ravishankara, *Science* **2006**, *311*, 67–70.
23. C. J. Gaston, J. A. Thornton, *J. Phys. Chem. A*. **2016**, *120*, 1039–1045.
24. C. B. Faxon, D. T. Allen, *Environ. Chem.* **2013**, *10*, 221–233.
25. T. P. Riedel, G. M. Wolfe, K. T. Danas, J. B. Gilman, W. C. Kuster, D. M. Bon, A. Vlasenko, S.-M. Li, E. J. Williams, B. M. Lerner, P. R. Veres, J. M. Roberts, J. S. Holloway, B. Lefer, S. S. Brown, J. A. Thornton, *Atmos. Chem. Phys.* **2014**, *14*, 3789–3800.
26. I. S. A. Isaksen, T. K. Berntsen, S. B. Dalsoren, K. Eleftheratos, Y. Orsolini, B. Rognerud, F. Stordal, O. A. Sovde, C. Zerefos, C. D. Holmes, *Atmosphere (Basel).* **2014**, *5*, 518–535.
27. L. M. Cosman, A. K. Bertram, *J. Phys. Chem. A*. **2008**, *112*, 4625–4635.
28. O. S. Ryder, N. R. Campbell, M. Shaloski, H. Al-Mashat, G. M. Nathanson, T. H. Bertram, *J. Phys. Chem. A*. **2015**, *119*, 8519–8526.
29. M. A. Shaloski, J. R. Gord, S. Staudt, S. L. Quinn, T. H. Bertram, G. M. Nathanson, *J. Phys. Chem. A*. **2017**, *121*, 3708–3719.

30. J. R. Gord, X. Zhao, E. Liu, T. H. Bertram, G. M. Nathanson, *J. Phys. Chem. A*. **2018**, *122*, 6593–6604.
31. T. B. Sobyra, H. Pliszka, T. H. Bertram, G. M. Nathanson, *J. Phys. Chem. A*. **2019**, *123*, 8942–8953.
32. W. Behnke, C. George, V. Scheer, C. Zetzsch, *Geophys. Res. Atmos.* **1997**, *102*, 3795–3804.
33. F. Schweitzer, P. Mirabel, C. George, *J. Phys. Chem. A* **1998**, 102, 3942-3952.
34. J. A. Thornton, C. F. Braban, J. P. D. Abbatt, *Phys. Chem. Chem. Phys.* **2003**, *5*, 4593.
35. V. F. McNeill, J. Patterson, G. M. Wolfe, J. A. Thornton, *Atmos. Chem. Phys.* **2006**, *6*, 1635–1644.
36. D. J. Stewart, P. T. Griffiths, R. A. Cox, *Atmos. Chem. Phys.* **2004**, *4*, 1381–1388.
37. C. George, J. L. Ponche, P. Mirabel, W. Behnke, V. Scheer, C. Zetzsch, *J. Phys. Chem.* **1994**, *98*, 8780–8784.
38. D. J. Donaldson, V. Vaida, *Chem. Rev.* **2006**, *106*, 1445–1461.
39. O. S. Ryder, N. R. Campbell, H. Morris, S. Forestieri, M. J. Ruppel, C. Cappa, A. Tivanski, K. Prather, T. H. Bertram, *J. Phys. Chem. A*. **2015**, *119*, 11683–11692.
40. P. J. Kelleher, F. S. Menges, J. W. DePalma, J. K. Denton, M. A. Johnson, G. H. Weddle, B. Hirshberg, R. B. Gerber, *J. Phys. Chem. Lett.* **2017**, *8*, 4710–4715.
41. A. F. Voegele, C. S. Tautermann, T. Loertingy, K. R. Liedl, *Phys. Chem. Chem. Phys.* **2003**, *5*, 487–495.
42. B. Hirshberg, E. Rossich Molina, A. W. Gotz, A. D. Hammerich, G. M. Nathanson, T. H. Bertram, M. A. Johnson, R. B. Gerber, *Phys. Chem. Chem. Phys.* **2018**, *20*, 17961–17976.
43. A. D. Hammerich, B. J. Finlayson-Pitts, R. B. Gerber, *Phys. Chem. Chem. Phys.* **2015**, *17*, 19360–19370.
44. D. Hanway, F.-M. Tao, *Chem. Phys. Lett.* **1998**, *285*, 459–466.
45. J. P. McNamara, I. H. Hillier, *J. Phys. Chem. A*. **2000**, *104*, 5307–5319.
46. J. R. Durig, Y. H. Kim, G. A. Guirgis, J. K. McDonald, *Spectrochim. Acta Part A Mol. Spectrosc.* **1994**, *50*, 463–472.
47. L. Martínez, R. Andrade, E. G. Birgin, J. M. Martínez, *J. Comput. Chem.* **2009**, *30*, 2157–2164.
48. J.-D. Chai, M. Head-Gordon, *Phys. Chem. Chem. Phys.* **2008**, *10*, 6615.
49. R. A. Kendall, T. H. Dunning, R. J. Harrison, *J. Chem. Phys.* **1992**, *96*, 6796.
50. D. E. Woon, T. H. Dunning, *J. Chem. Phys.* **1993**, *98*, 1358–1371.
51. A. E. DePrince, C. D. Sherrill, *J. Chem. Theory Comput.* **2013**, *9*, 293–299.
52. A. E. DePrince, C. D. Sherrill, *J. Chem. Theory Comput.* **2013**, *9*, 2687–2696.
53. U. Bozkaya, *J. Chem. Phys.* **2016**, *144*, 144108.
54. K. Fukui, *J. Phys. Chem.* **1970**, *74*, 4161–4163.
55. E. D. Glendening, C. R. Landis, F. Weinhold, *J. Comput. Chem.* **2019**, *40*, 2234–2241.
56. F. Weinhold, C. R. Landis, E. D. Glendening, *Int. Rev. Phys. Chem.* **2016**, *35*, 399–440.
57. Y. Shao *et al.*, *Mol. Phys.* **2015**, *113*, 184–215.
58. R. M. Parrish, L. A. Burns, D. G. A. Smith, A. C. Simmonett, A. E. DePrince, III, E. G. Hohenstein, U. Bozkaya, A. Y. Sokolov, R. DiRemigio, R. M. Richard, J. F. Gonthier, A. M. James, H. R. McAlexander, A. Kumar, M. Saitow, X. Wang, B. P. Pritchard, P. Verma, H. F. Schaefer, III, K. Patkowski, R. A. King, E. F. Valeev, F. A. Evangelista, J. M. Turney, T. D. Crawford, C. D. Sherrill, *J. Chem. Theory Comput.* **2017**, *13*, 3185–3197.

Entry for the Table of Contents

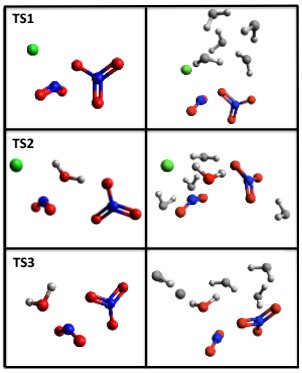

TOC: Left: Substructure references from smallest clusters that contain the TS motif. Right: highlighted substructures in lowest barrier n=5 clusters. Top: TS1 corresponds to the $N_2O_5/Cl^{\delta-}/nH_2O \rightarrow ClNO_2/NO_3^{\delta-}/nH_2O$ reaction; Middle: TS2 corresponds to the $ClNO_2/NO_3^{\delta-}/nH_2O \rightarrow HNO_3/NO_3^{\delta-}/HCl/(n-1)H_2O$ reaction; Bottom: TS3 corresponds to the $N_2O_5/Cl^{\delta-}/nH_2O \rightarrow HNO_3/NO_3^{\delta-}/HCl/(n-1)H_2O$ reaction.

Institute and/or researcher Twitter usernames: @laura_mccaslin, @SandiaLabs, @awgoetz, @YaleChem